JOURNAL OF UNDERGRADUATE RESEARCH

Magmatic and Tectonic Setting of Archean Granitoids in the Southeastern Singhbhum Craton, India: Developing constraints with major and trace element geochemistry and geochronology

Claudia Banks
University of Florida

Faculty Mentor: Joseph G. Meert, Department of Geological Sciences

Abstract

The Singhbhum craton is one of five Archean nuclei comprising peninsular India. It is a composite Archean block that includes the Older Metamorphic Group, the Older Metamorphic Tonalite Gneisses, the Singhbhum Granite, and the Iron Ore Group as its major units. The ages of these components range from ~3.5 to ~3.1 Ga, although overlapping ages and similar rock types confound their genetic relationships. Plutonic felsic rocks from the southeastern Singhbhum craton (BK1: a foliated tonalite, KP1: a non-foliated granite, and SG14: a non-foliated granite) yield U-Pb (zircon) ages of 3348 ± 20 Ma (BK1), 3172 ± 8 Ma (KP1), and 3243 ± 4 Ma (SG14) that coincide with a pulse of Singhbhum Granite emplacement at 3.27 to 3.33 Ga. REE patterns and tectonic discrimination diagrams based on major and trace element ratios suggest a subduction zone setting for these rocks. Major and trace element data are reported and compared to previous works to characterize the Archean felsic plutonic history of the craton.

Keywords: Granite, Singhbhum craton, Geochemistry, U-Pb system, zircon dating

Introduction

The Singhbhum craton (northeastern India, Figure 1) consists of four distinct groups of low grade metamorphic rocks and granitic batholiths: Older Metamorphic Tonalite Gneisses (OMTG; 3.8–3.1 Ga), the Older Metamorphic Group (OMG; 3.7–3.2 Ga), Iron Ore Group (IOG; 3.51–2.55 Ga), and Singhbhum Granite (3.5–3.0 Ga) (Miller et al., 2018). The OMTG consists of metamorphosed biotite-hornblende tonalites, trondhjemites, and granites (Baksi et al., 1987; Upadhyay et al., 2019). The OMTG rocks are enriched in light rare earth elements (LREE) and are moderately depleted in heavy rare earth elements (HREE) relative to chrondrites (Upadhyay et al., 2019). The OMTG was emplaced in two pulses, at 3.45–3.44 Ga and 3.35–3.32 Ga, and intrudes the OMG, which consists of pelitic schists and amphibolite that have a LREE enrichment relative to chondrites and an age range of 3.20-3.63 Ga (Saha, 1994; Upadhyay et al.,

2019). The IOG is comprised of low-grade metasedimentary and metavolcanics rocks along with banded iron formations. The IOG is distributed throughout the craton in three regions known as the western, eastern, and southern IOG. Dacitic lavas in the southern IOG are dated at 3507 ± 2 Ma (Mukhopadhyay et al., 2008). Geochronologic data from the other IOG basins are sparse, so the range of depositional ages is not clear (Upadhyay et al., 2019). The Singhbhum Granite is a batholith that covers an area of about 10,000 km^2 and is the nucleus the craton. The Singhbhum Granite consists of granodiorite-trondhjemites and K-rich granodiorites to monzogranites (Saha, 1994; Dey et al., 2017). Saha (1994) suggested this batholith is made of about 12 magmatic bodies that were emplaced in three phases. Phase I is composed of granodiorite-trondhjemites while Phase II and Phase III consist of K-rich granodiorites to monzogranites. The largest bodies are composed of the K-rich granodiorites and monzonites. All three phases show an enrichment of Li, Sr, and Ni and a depletion in Mn, Ba, and Y relative to the average granite (Saha, 1994). The Singhbhum granites are enriched in LREE with negative Eu anomalies (Upadhyay et al., 2019). Saha (1994) argues an emplacement age of about 3.3 Ga for Phase I and II and that these phases formed as the result of partial melting of amphibolite at the base of the crust while Phase III has an age of about 3.1 Ga and resulted from partial melting of the crust. Dey et al. (2017) argues that the evidence for multi-phase emplacement is weak because the ages of the granitoids overlap. The rocks comprising the Singhbhum craton were subsequently deformed and metamorphosed at 3.30–3.28 Ga, 3.19–3.13 Ga and 3.02–2.96 Ga (Saha, 1994; Mukhopadhyay, 2001; Upadhyay et al., 2019). Other geochemical studies conducted on different rocks in the craton further facilitates a subduction zone setting for the craton. Manikyamba et al. (2015) studied boninites (OMG) collected from the central/northwestern section of the craton. The boninites' HFSE composition indicate melting of mantle wedge peridotite. Boninite formation also occurs during the early stages of subduction when the subducting slab begins dehydrating and mantle wedge metasomatism occurs, leading to the formation of boninites. Mafic dikes in the Singhbhum craton also have a subduction zone geochemical signature. According to Mir et al. (2015), mafic dike samples from the central part of the Singhbhum craton featured LREE and LILE enrichment, negative Nb, U, Sr, and Ti anomalies; all of which are characteristic of subduction-related back arc extensional basalts.

Globally, the general tectonic setting of Eoarchean to Paleoarchean age crust is disputed. Polat et al. (2016) and Kaczmarek et al. (2016) advocate for a subduction setting. Polat et al.

(2016) examined > 3.0 Ga TTG gneisses in the Tartoq greenstone belt (Greenland) and concluded that thick buoyant crust formed subduction-accretion complexes in that region. This argument was based on density modeling, isotopic, and trace element compositions. According to the model advocated by Polat et al. (2016), convergent margins were active by 3.8 Ga, and oceanic crust was thicker and less dense than its modern counterparts. The lighter, more buoyant oceanic crust was unsubductable and formed accreted plates in the Archean. Partial melting of subduction-created crust may have been significant in creating continental crust in the Archean. Kaczmarek et al. (2016) suggests that subduction was active in the Eoarchean based on preferred alignment of olivine crystals (B-type fabrics) in Greenland. The orientation of B-type fabrics indicates deformation of mantle rocks in the hanging wall of subducting crust (Kaczmarek et al., 2016). In contrast to the above models, Van Kranendonk et al. (2015), Johnson et al. (2017), and Asokan et al. (2020) argue against a subduction zone setting for Archean crust in favor of an oceanic plateau setting. Instead of the shallow subduction model, tonalite-trondhjemite-granodiorite (TTG) continental crust is created from mantle plumes, forming oceanic plateaus or large igneous provinces (Van Kranendonk et al., 2015). Johnson et al. (2017) supports the idea that Archean-aged TTG rocks formed from partial melting of thick basaltic crust and that arc signatures in trace elements were derived from an ancestral basalt lineage. Asokan et al. (2020) examined granitic samples in the Singhbhum craton and argued that they formed in an oceanic environment. Overall, the tectonic setting of formation and the classification of the dozen or so, Singhbhum magmatic pulses are not well constrained, therefore, this study aims to provide more information on the formation of Paleoarchean continental crust by analyzing geochemical/geochronological signals of the Singhbhum Craton and comparing with the previous work such as Dey et al. (2017), Upadhyay et al. (2019), and Asokan et al. (2020).

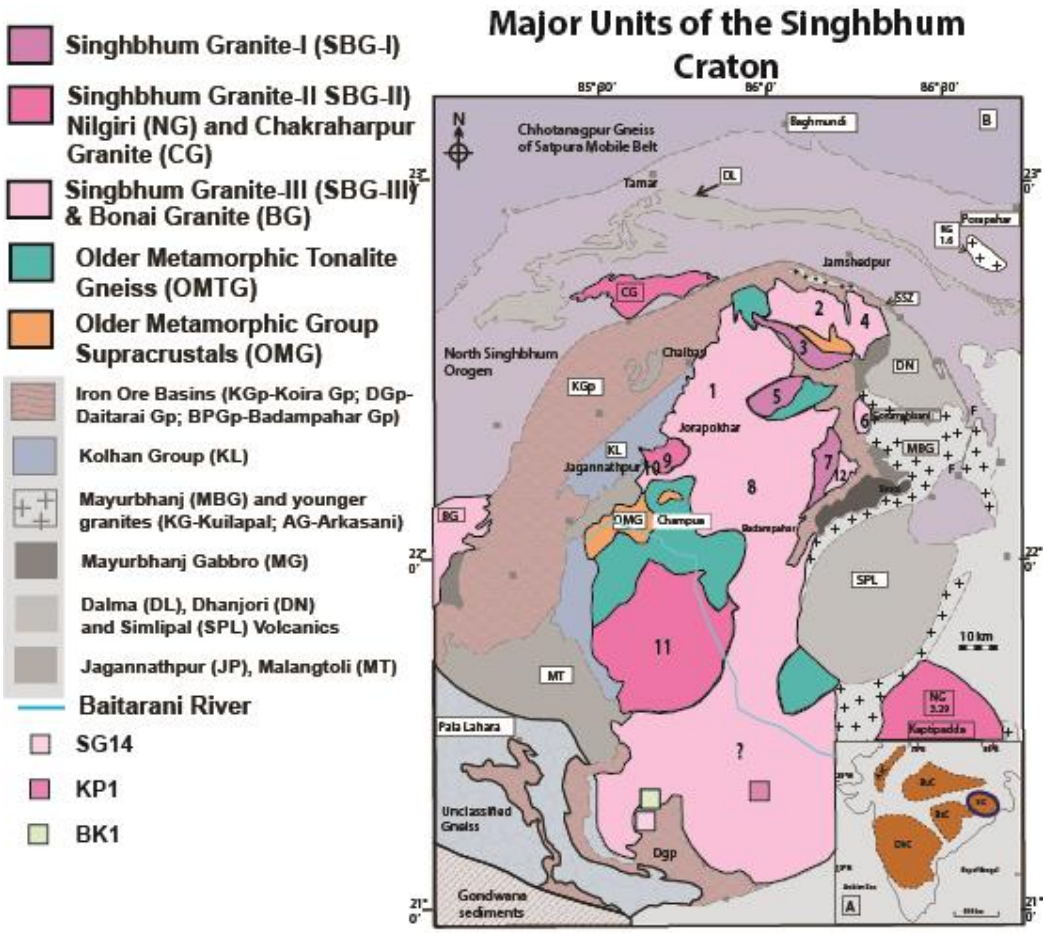

Figure 1. A geologic map of the Singhbhum craton located in eastern India (modified after Saha, 1994). The locations of the study area are depicted with squares. The craton is believed to have formed from 12 magmatic pulses as depicted by the numbers 1-12 in the figure. The insert shows the location of other cratons in India.

Methods

Three granitoid samples were collected from the Singhbhum Granite and OMTG in the southernmost Singhbhum craton (Figure 1). Modal mineralogy for the tonalite (BK1) and one of the granites (KP1) was determined from thin sections that were cut and studied under an optical microscope. For geochemical analyses, rocks were crushed to a fine powder (<50 mm) with a jaw crusher and puck mill. Major element analyses were determined with fused glass beads via X-ray fluorescence (XRF). Trace elements were analyzed with Inductively Coupled Plasma-Mass Spectrometry (ICP-MS). For geochronology, the three rock samples were cut, milled, and sieved to retrieve zircon grains <300 μm. After washing, non-magnetic grains were separated using a magnetic separator (Frantz LB-1 Magnetic Barrier Laboratory Separator) and zircons were then separated from lighter grains using heavy liquid settling techniques. Individual zircons

were hand-picked under a binocular microscope and placed in epoxy resin with FC-1 zircon standard. Individual zircons were examined with scanning electron microscopy (SEM) to obtain backscatter electron (BSE) and cathodoluminescence (CL) images. Zircons were examined via analysis of $^{207}Pb/^{206}Pb$ ratios for individual zircon mineral grains with a Nu Plasma II Laser Ablation-Inductively Coupled Plasma Mass Spectrometry (LA-ICP-MS) system. U-Pb age data were reduced with the CALAMARI program (© Mueller, 2014). Zircons with a $^{207}Pb/^{206}Pb$ discordance <5% were plotted on concordia diagrams created with the program IsoplotR (Vermeesch, 2018).

Analytical Results

Geochronology

The weighted mean ages from BK1, KP1, and SG14 range from 3172-3348 Ma. Five grains from BK1 yielded a concordant age of 3275 ± 5 Ma (MSWD = 4.3) (Figure 2a). Seven concordant grains from sample KP1 yield an age of 3290 ± 2 Ma (MSWD = 13) (Figure 2b). Five zircons from SG14 yielded a concordant of 3275 ± 5 Ma (MSWD = 4.3) (Figure 2c). In contrast, sample BK1 yielded a discordia upper intercept of 3348 ± 20 Ma and a lower intercept of 861 ± 5 Ma. Sample KP1 yielded a discordia with an upper intercept age of 3172 ± Ma and a lower intercept at 534 ± 5 Ma. Sample SG14 yielded a discordia with a lower intercept at 519 ± 3 Ma and an upper intercept of 3243 ± 4 Ma. The upper intercept ages are slightly different than the concordant ages cited above. The differences may be attributed to systematic Pb-loss during subsequent metamorphism and uplift. BK1 zircons are anhedral and display no zoning (Figure 3a). KP1 zircons are anhedral with oscillatory zoning observed in CL images (Figure 3b). SG14 zircons exhibit oscillatory zoning and a subhedral shape (Figure 3c).

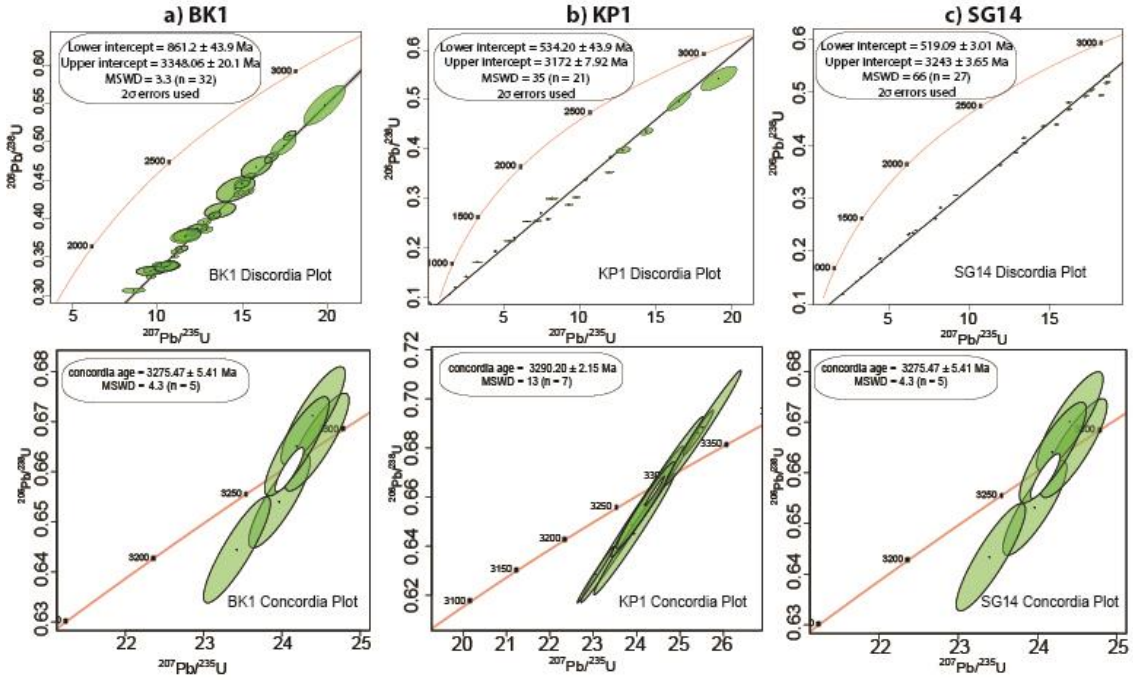

Figure 2. U-Pb Concordia and Discordia plots for the zircons from BK1, SG14, and KP1.

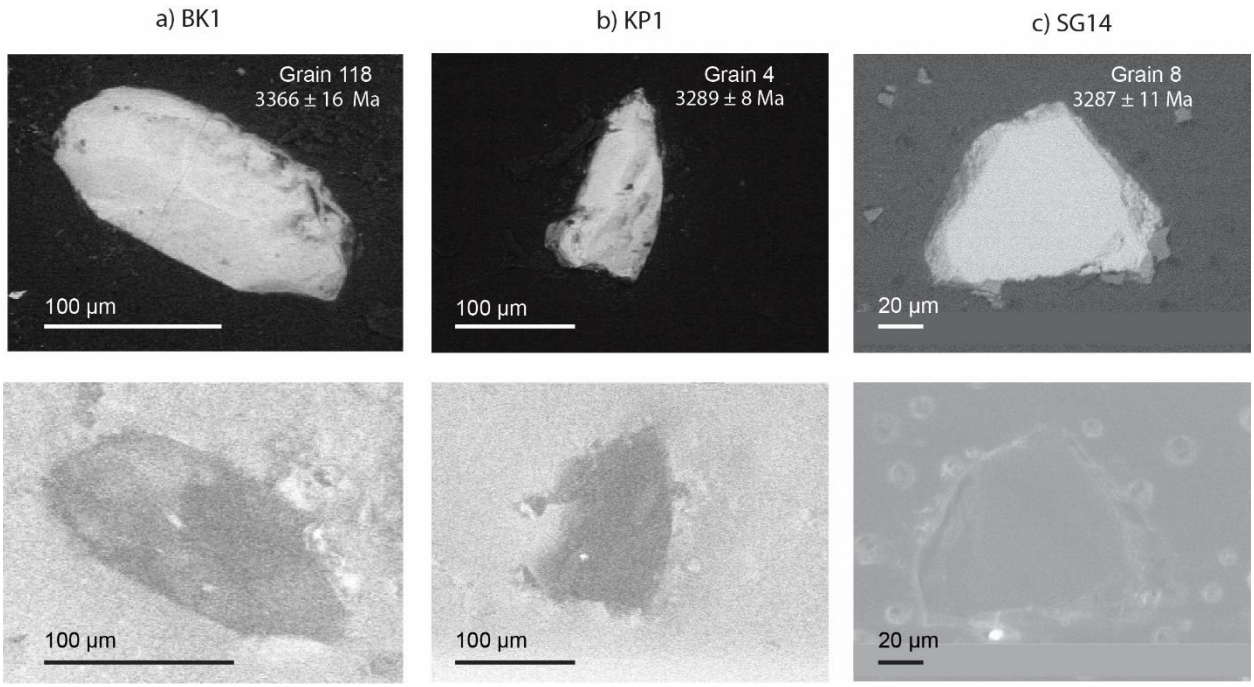

Figure 3. SEM images of zircons <300 *µm* collected from samples BK1, SG14, and KP1. CL images are displayed on the bottom row and BSE images are shown on the top row.

Petrography this section should precede the age paragraphs

BK1 contains tartan twined K-feldspar (5%) hornblende (5%), biotite (5%), quartz (35%), and plagioclase (50%) (Figure 4a and Figure 4b). KP1 contains twined K-feldspar (30%), biotite (5%), chlorite (5%), quartz (40%), and plagioclase (20%) (Figure 4c and Figure 4d). K-spar is translucent and displays microcline twinning and 90° cleavage. Plagioclases in both samples are translucent/grey with 90° cleavage and simple twinning. BK1 also exhibits hornblende and biotite. Biotite in BK1 displays green/brown color and characteristic birds eye extinction. Hornblende is green with 60-120° cleavage and is present only in BK1. Both KP1 and BK1 exhibit sericitization of plagioclase.

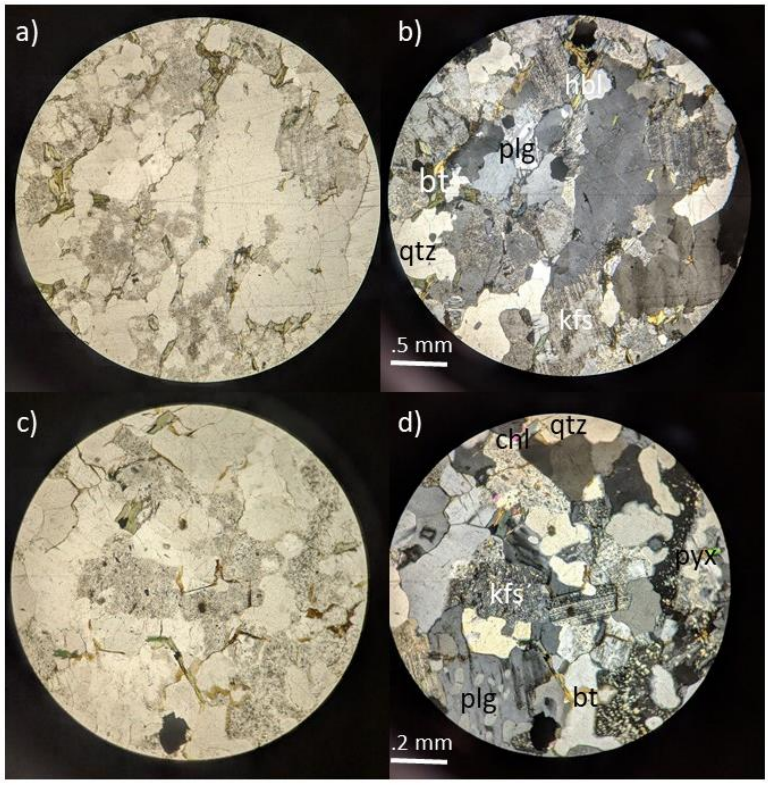

Figure 4. a) BK1 in ppl and b) BK1 in xpl is classified as a tonalite. Fig c) KP1 in ppl and d) KP1 in xpl is classified as a granite. (ppl, plane light; xpl, crossed polarized light).

Major/trace elements

The plutonic TAS total alkali-silica ($Na_2O + K_2O$ vs SiO_2) plot classifies the samples KP1 and SG14 as granites and BK1 as a tonalite, respectively (Middlemost, 1994) (Figure 6). KP1 and SG14 show a high silica content at 73.89 and 74.78 wt. %. They also demonstrate a moderate total alkali content of 7.39 to 8.10. BK1 has a moderate to low silica content at 61.11

wt. % and a low total alkali content of 5.65. Based on iron and magnesium content, the granites are ferroan with a high SiO_2 wt. % and a FeO / (FeO + MgO) of 0.86 (KP1) to 0.91 (SG14) (Figure 7b). BK1 is between ferroan and magnesian composition FeO / (FeO + MgO) wt. % 0.77 (Frost et al., 2008) (Figure 7b). The modified alkali-lime index ($Na_2O + K_2O – CaO$) vs SiO_2 diagrams depict the KP1 as alkalic-calcic (7.41 $Na_2O + K_2O – CaO$), while SG14 and BK1 are less potassic calc-alkalic rocks (6.13 $Na_2O + K_2O – CaO$ and 1.03 $Na_2O + K_2O – CaO$, respectively; Frost et al., 2001; Figure 7a).

The chondrite normalized rare earth element (REE) plot of the three samples show a fractionated LREE, flat HREEs and a negative Eu anomaly (Figure 8a). BK1 shows low normalized values of Ce and La while KP1 and SG14 exhibit higher values. KP1 has a high enrichment of LREE with Ce and La. SG14 has moderately enriched LREE relative to BK1 and KP1. The slopes of REE patterns are described by their La/Yb ratios. La/Yb ratios are negative in KP1 and SG14, which indicates the accumulation of plagioclase during shallow level crystallization of the granite pluton. Overall, BK1 has a higher HREE and a lower LREE relative to KP1 and SG14. The primitive mantle normalized extended trace element plot shows an enrichment in large ion lithophiles (LILE; Ca and Rb), Th, U, and Pb, while there is a significant depletion in the high field strength element (HFSE) Nb, which is exhibited in BK1, KP1, and SG14 (Figure 8b). BK1 displays a pattern similar to tonalites recorded by Dey et al. (2017) in both chondrite normalized and primitive mantle normalized plots. KP1 and SG14 also exhibit similar patterns and anomalies as the non-porphyritic granites of Asokan et al. (2020), Upadhyay et al. (2019) and Dey et al. (2017).

Figure 9 displays the tectonic setting discrimination diagrams on which non-porphyritic granites, porphyritic granites, tonalites/trondhjemites from Dey et al. (2017), Upadhyay et al. (2019), Asokan et al. (2020) and this study have been plotted. Figure 9a (Hollocher et al., 2012) displays La/Yb ratios against Th/Nb ratios. Most data for all studies plot in the alkaline arcs section due to relatively high La/Yb and Th/Nb ratios. BK1 plots under oceanic island due to a relatively moderate La/Yb and low Th/Nb ratios. The tonalite from Dey et al. (2017) is classified under a continental arc setting from a high Th/Nb ratio, but moderate La/Yb ratio. Figure 9b plots Yb (ppm) vs Ta (ppm). Samples of Asokan et al. (2020) and Upadhyay et al. (2019) plot in the syn-collisional granites and volcanic arc granites field. BK1, KP1, and SG14 are all categorized under volcanic arc granites.

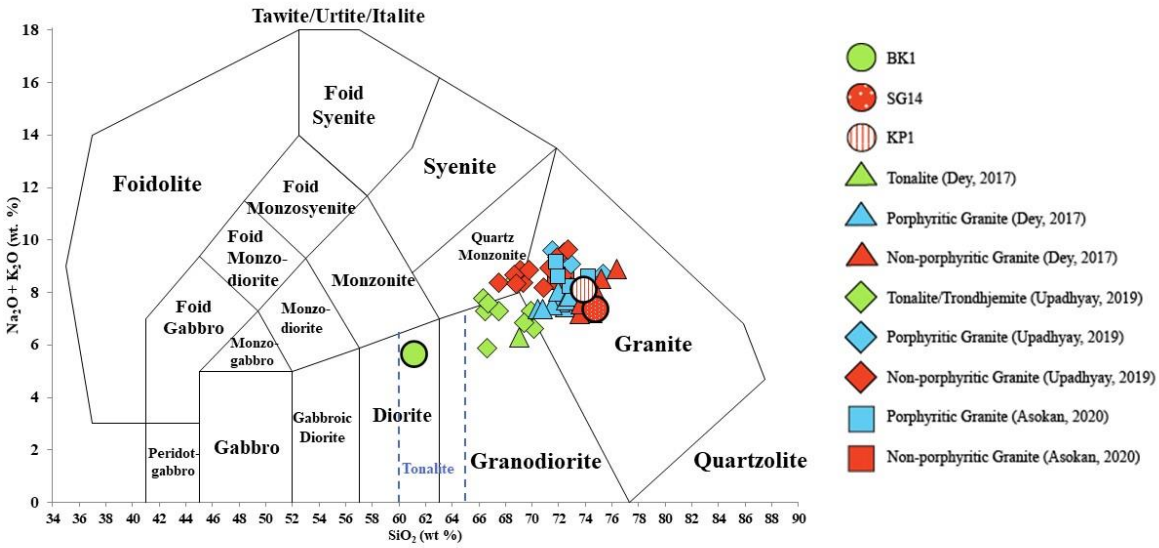

Figure 6. BK1 is classified as a tonalite while KP1 and SG14 are classified as granites. According to Middlemost (1994), the silica content range for a tonalite is between 60 and 65 wt. %.

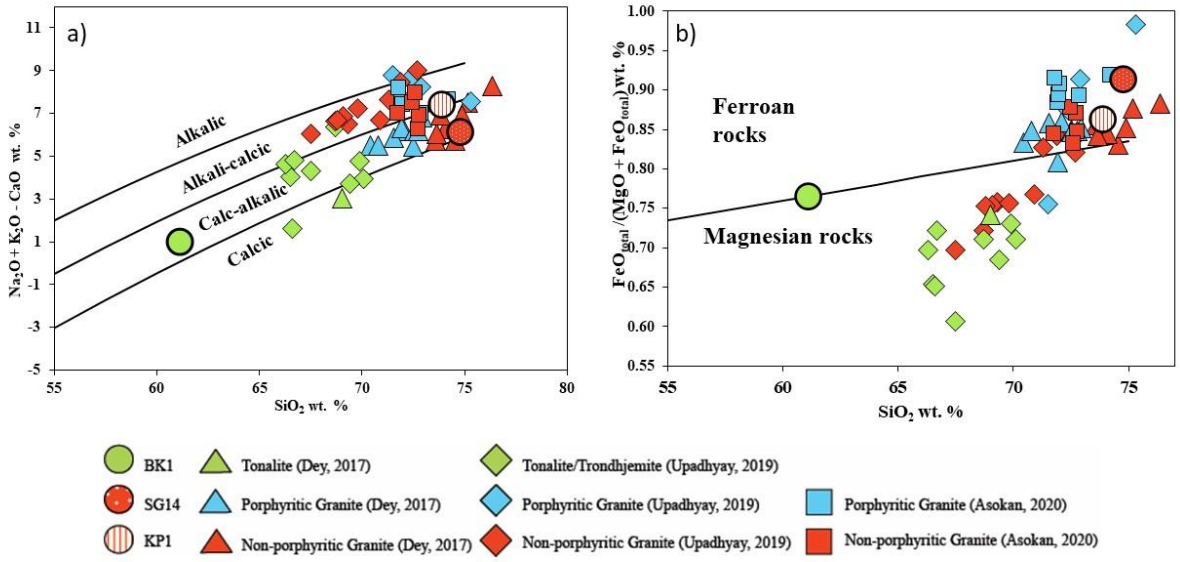

Figure 7. a) Modified alkali lime index used to classify granitic rocks based on sodium, potassium, and calcium content (Frost et al., 2001). b) A classification for feldspathic igneous rocks based on magnesium and iron content (Frost et al., 2008)

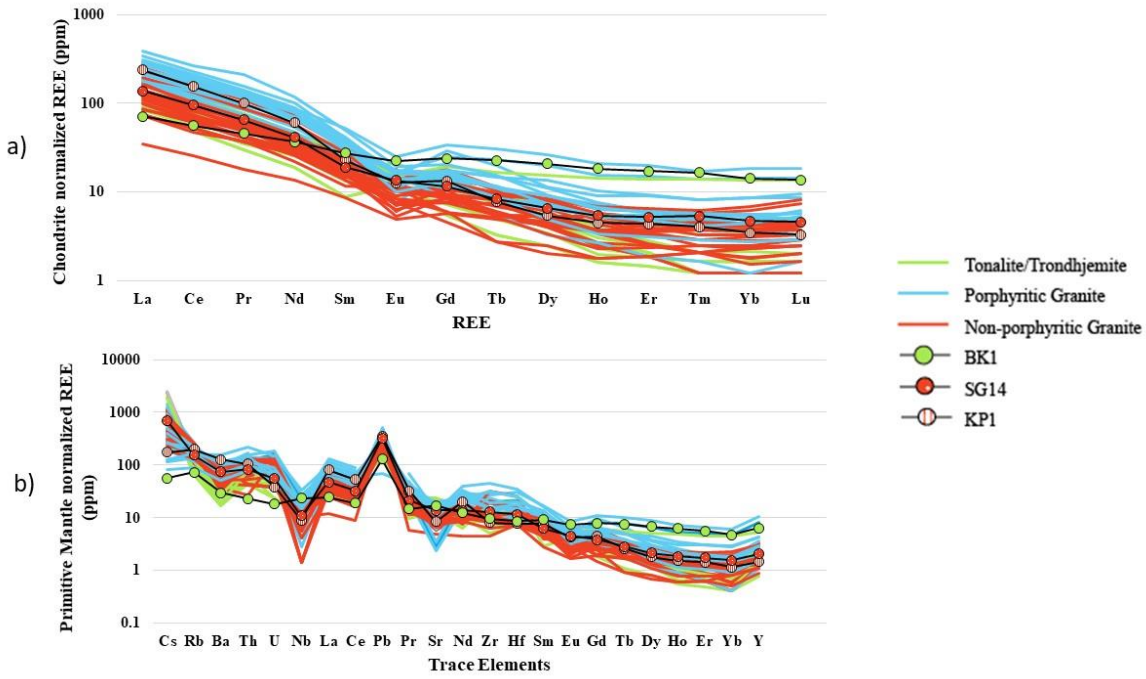

Figure 8. a) Chondrite normalized REE patterns. b) Primitive Mantle normalized extended trace element plot.

Discussion

This study explores three samples; two granites (SG14 and KP1) and one tonalite (BK1); in the southernmost Singhbhum craton. Asokan et al. (2020) also collected samples from the southern part of the Singhbhum craton. Other samples from Dey et al (2017) and Upadhyay et al. (2019) were collected from the central part of the craton. Overall, the results in this study support the findings of Dey et al. (2017), Upadhyay et al. (2019), and Asokan et al. (2020); however, there are slight variations between rock types.

The age distribution (3.17-3.35 Ga) of the zircons in the tonalite (BK1) and granites (SG14 and KP1) match the age of the proposed second pulse of emplacement of the Singhbhum Granite (3.27-3.33 Ga). The presence of chlorite in KP1 indicates some post-crystallization alteration. Textures in both KP1 and BK1 thin sections include sericitization of plagioclase, which typically occurs during hydrothermal alteration (Dey et al., 2017). BK1, SG14, and KP1 generally yield similar REE patterns with a few key differences. The granites (KP1 and SG14) show negative Eu anomalies in contrast to the tonalite (BK1). BK1 is more enriched and less depleted relative to primitive mantle whereas the granites are more enriched relative to primitive mantle. In previous publications, most HREE patterns are consistently reported as depleted relative to LREE for the

second pulse of emplacement and flat for the ~3.1 Ga pulse, whereas LREE abundances are more variable (Upadhyay et al., 2019).

The petrogenesis of the Singhbhum craton melts was previously attributed to a variety of mechanisms, including melting of subducted MORB-like oceanic crust, subduction of oceanic plateaus, and melting of wet basalts at the base of oceanic plateaus (Nair and Chacko, 2008; Polat, 2012; Martin et al., 2014; Upadhyay et al., 2019; Asokan et al., 2020). The presence of negative Eu and Sr anomalies indicate a shallow crustal source for the granites (Upadhyay, 2019). In the primitive mantle normalized trace element plot, there is a large depletion in Nb, and an enrichment in Pb (Zheng, 2019). The depletion in Nb indicates a subduction zone setting because it is a HFSE. HFSEs have a higher charge and are immobile in fluids present in subduction zones so they remain in the solid. Pb is a LILE, meaning it has a lower charge and is fluid-mobile, so it does not remain in the solid, explaining its enrichment in the trace element plot (Zheng, 2019). Asokan et al. (2020) argues these anomalies are not enough evidence for a subduction zone setting and can instead infer mantle plume interaction with continental crust due to similar geochemical patterns (Condie, 2005; Rudnick & Fountain, 1995).

Based on our analyses, both SG14 and BK1 formed in a calc-alkaline subduction setting. KP1 is classified as an alkali-calcic, suggesting its formation in an anorogenic setting (Hollocher et al., 2012) (Figure 11). Dey et al. (2017) collected porphyritic and non-porphyritic granites from the eastern side of the Singhbhum craton. The majority of granites from Dey et al. (2017) are silica-rich, calc-alkalic, and ferroan. Dey et al. (2017) reported an age of 3311 ± 57 Ma for the non-porphyritic granites. Upadhyay et al (2019) interpreted trondhjemites and tonalite as magnesian, calcic to calc-alkalic rocks that are enriched in LREE and depleted in HREE with minor Eu anomalies. Granites from Upadhyay et al. (2019) are alkali-calcic to alkalic and ferroan and magnesian. HREE are depleted and REE patterns are fractionated. Eu anomalies in REE patterns are negative. U-Pb ages of Upadhyay et al. (2019) samples range from 3.05-3.45 Ga.

All samples in this study (BK1, KP1, and SG14) classify as volcanic arc granites. Pearce et al. (1984) notes that volcanic arc granites' setting can vary from continental to oceanic. The composition of these granites can also vary from calc-alkalic to tholeiitic. According to the discrimination diagram created by Hollocher et al. (2016), KP1 and SG14 formed in an alkaline arc setting. SG14 and KP1's compositions match the Asokan et al. (2020), Upadhyay et al. (2019), and Dey et al. (2017) non-porphyritic granites. However, the tonalites in all studies have different settings. The tonalite from Upadhyay et al. (2019) is classified under alkaline arc while the tonalite from Dey et al. (2017) plots under continental arc.

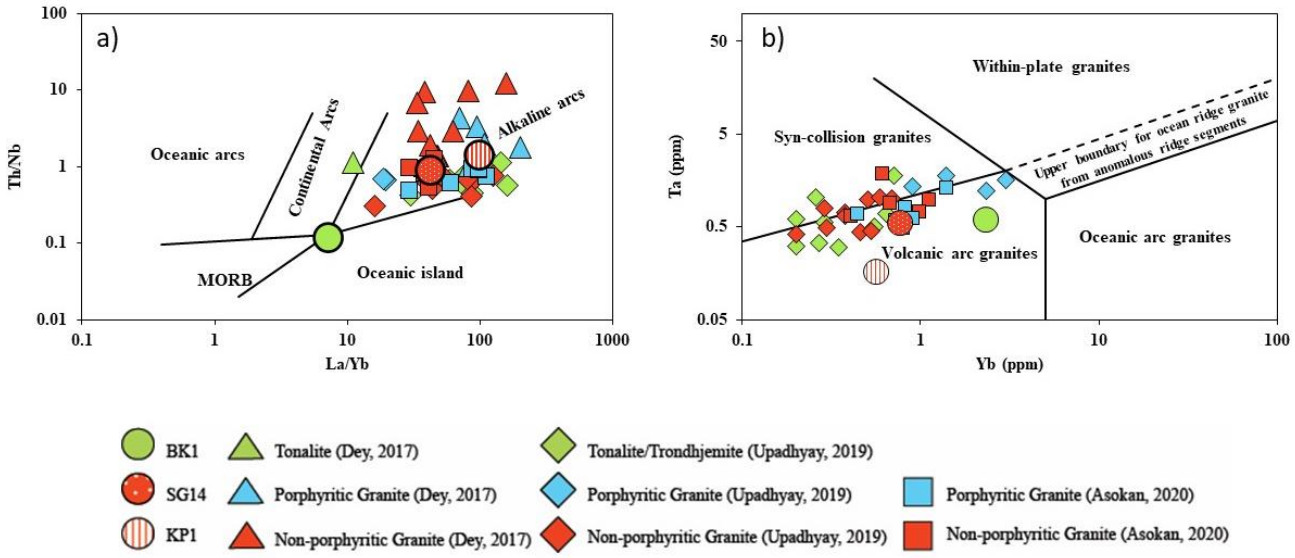

Figure 9. a) Tectonic discrimination diagram from Hollocher et al. (2012). b) Tectonic discrimination from Pearce et al. (1984).

Conclusion

Three samples were collected from the Singhbhum Granite batholith complex. LA-ICP MS U-Pb zircon yielded an age range of ~3.26-3.34 Ga for these samples. Sample BK1 was classified as tonalite and is from the OMTG. Zircons from this sample have an average U-Pb age of 3348 ± 20 Ma. KP1 and SG14 were classified as granites. KP1 yielded an age 3172 ± 8 Ma. SG14 has an age of 3243 ± 4 Ma. BK1's unique composition likely represents an enclave in the younger Singhbhum granitoids. These ages correspond to a pulse of Singhbhum Granite emplacement at 3.27 to 3.33 Ga. Samples were compared to Dey et al. (2017), Upadhyay et al.

(2019), and Asokan et al. (2020) tonalite, trondhjemites, and granites (porphyritic and non-porphyritic). The anomalies in the spider diagrams and the tectonic discrimination diagrams indicate a volcanic arc setting or convergent margin setting. The argument for a subduction zone setting for the craton is often disputed because the presence and rate of plate tectonics in the Archean is still not completely agreed on. This study compared the chemical and chronological signatures of the Singhbhum Granite with previous works such as Dey et al. (2017), Upadhyay et al. (2019), and Asokan et al. (2020) to better understand the formation of Archean continental crust.

Acknowledgements

Part of this work was supported by an EAR18-50693 and EAR13-47942 from the US National Science Foundation to JGM. The conclusions represent those of the authors and not the funding agency.

References

Asokan, A.D., Krishna, K., Elangovan, R. and Mohan, M.R., 2020. Petrogenesis of the Palaeoarchean Keonjhar Granite, Singhbhum Craton, India: product of crustal reworking or subduction? *Current Science*, *118*(6), 910.

Baksi, A.K., Archibald, D.A., Sarkar, S.N. and Saha, A.K., 1987. 40Ar–39Ar incremental heating study of mineral separates from the early Archean east Indian craton: implications for the thermal history of a section of the Singbhum Granite batholithic complex. *Canadian Journal of Earth Sciences*, *24*(10), 1985-1993.

Condie, K.C., 2005. High field strength element ratios in Archean basalts: a window to evolving sources of mantle plumes? *Lithos*, *79*(3-4), 491-504.

Dey, S., Topno, A., Liu, Y. and Zong, K., 2017. Generation and evolution of Palaeoarchaean continental crust in the central part of the Singhbhum craton, eastern India. *Precambrian Research*, *298*, 268-291.

Frost, B.R., Barnes, C.G., Collins, W.J., Arculus, R.J., Ellis, D.J. and Frost, C.D., 2001. A geochemical classification for granitic rocks. *Journal of Petrology*, *42*(11), 2033-2048.

Frost, B.R. and Frost, C.D., 2008. A geochemical classification for feldspathic igneous rocks. *Journal of Petrology*, *49*(11), 1955-1969.

Hollocher, K., Robinson, P., Walsh, E. and Roberts, D., 2012. Geochemistry of amphibolite-facies volcanics and gabbros of the Støren Nappe in extensions west and southwest of Trondheim, Western Gneiss Region, Norway: a key to correlations and paleotectonic settings. *American Journal of Science*, *312*(4), 357-416.

Johnson, T.E., Brown, M., Gardiner, N.J., Kirkland, C.L. and Smithies, R.H., 2017. Earth's first stable continents did not form by subduction. *Nature, 543*(7644), 239-242.

Kaczmarek, M.A., Reddy, S.M., Nutman, A.P., Friend, C.R. and Bennett, V.C., 2016. Earth's oldest mantle fabrics indicate Eoarchaean subduction. *Nature Communications, 7*(1), 1-7.

Manikyamba, C., Ray, J., Ganguly, S., Singh, M.R., Santosh, M., Saha, A. and Satyanarayanan, M., 2015. Boninitic metavolcanic rocks and island arc tholeiites from the Older Metamorphic Group (OMG) of Singhbhum Craton, eastern India: Geochemical evidence for Archean subduction processes. *Precambrian Research, 271*, 138-159.

Martin, H., Moyen, J.F., Guitreau, M., Blichert-Toft, J. and Le Pennec, J.L., 2014. Why Archaean TTG cannot be generated by MORB melting in subduction zones. *Lithos, 198*, 1-13.

Middlemost, E.A., 1994. Naming materials in the magma/igneous rock system. *Earth-Science Reviews, 37*(3-4), 215-224.

Miller, S.R., Mueller, P.A., Meert, J.G., Kamenov, G.D., Pivarunas, A.F., Sinha, A.K. and Pandit, M.K., 2018. Detrital zircons reveal evidence of Hadean crust in the Singhbhum Craton, India. *Journal of Geology, 126*(5), 541-552.

Mir, A.R., Alvi, S.H. and Balaram, V., 2010. Geochemistry of mafic dikes in the Singhbhum Orissa craton: implications for subduction-related metasomatism of the mantle beneath the eastern Indian craton. *International Geology Review, 52*(1), 79-94.

Mukhopadhyay, D., 2001. The Archaean nucleus of Singhbhum: the present state of knowledge. *Gondwana Research, 4*(3), 307-318.

Mukhopadhyay, J., Beukes, N.J., Armstrong, R.A., Zimmermann, U., Ghosh, G. and Medda, R.A., 2008. Dating the oldest greenstone in India: a 3.51-Ga precise U-Pb SHRIMP zircon age for dacitic lava of the southern Iron Ore Group, Singhbhum craton. *Journal of Geology, 116*(5), 449-461.

Nair, R. and Chacko, T., 2008. Role of oceanic plateaus in the initiation of subduction and origin of continental crust. *Geology, 36*(7), 583-586.

Pearce, J.A., Harris, N.B. and Tindle, A.G., 1984. Trace element discrimination diagrams for the tectonic interpretation of granitic rocks. *Journal of Petrology, 25*(4), 956-983.

Polat, A., 2012. Growth of Archean continental crust in oceanic island arcs. *Geology, 40*(4), 383-384.

Polat, A., Kokfelt, T., Burke, K.C., Kusky, T.M., Bradley, D.C., Dziggel, A. and Kolb, J., 2016. Lithological, structural, and geochemical characteristics of the Mesoarchean Târtoq greenstone belt, southern West Greenland, and the Chugach–Prince William accretionary complex, southern Alaska: evidence for uniformitarian plate-tectonic processes. *Canadian Journal of Earth Sciences, 53*(11), 1336-1371.

Rudnick, R.L. and Fountain, D.M., 1995. Nature and composition of the continental crust: a lower crustal perspective. *Reviews of Geophysics, 33*(3), 267-309.

Saha, A.K., 1994. Crustal Evolution of Singhbhum North Orissa Eastern India. *Mem. Geolog. Soc. India*.

Upadhyay, D., Chattopadhyay, S. and Mezger, K., 2019. Formation of Paleoarchean-Mesoarchean Na-rich (TTG) and K-rich granitoid crust of the Singhbhum craton, eastern India: Constraints from major and trace element geochemistry and Sr-Nd-Hf isotope composition. *Precambrian Research, 327*, 255-272.

Van Kranendonk, M.J., Smithies, R.H., Griffin, W.L., Huston, D.L., Hickman, A.H., Champion, D.C., Anhaeusser, C.R. and Pirajno, F., 2015. Making it thick: a volcanic plateau origin of Palaeoarchean continental lithosphere of the Pilbara and Kaapvaal cratons. Geological Society, London, Special Publications, 389(1), 83-111.

Vermeesch, P., 2018. IsoplotR: A free and open toolbox for geochronology. *Geoscience Frontiers, 9*(5), 1479-1493.

Zheng, Y.F., 2019. Subduction zone geochemistry. *Geoscience Frontiers, 10*(4), 1223-1254.